

Figure S1. PRMT5 knockout in the fetal liver compartment leads to severe anemia, embryonic lethality, and impairs fetal erythropoiesis & cell cycle progression. Related to Figure 2. (A) Schematic of mouse *Prmt5* targeting strategy. **(B)** qRT-PCR analysis showing relative mRNA levels of *Prmt5* in *Prmt5*^{+/+} (WT), *Prmt5*^{+/fl} (HET), and *Prmt5*^{fl/fl} (KO) *Vav1-Cre*⁺ E14.5 FLCs. **(C)** Immunoblot with PRMT5 and GAPDH antibodies in *Prmt5* WT, HET and KO E14.5 FLCs. **(D)** Quantification of total cell numbers in PRMT5 WT, HET and KO E14.5 fetal livers. Error bars are SEM of at least 3 biological replicates. **** *P*<0.0001. N.S.: not significant **(E)** Representative picture of E16.5 PRMT5 WT vs KO embryos. **(F)** Flow cytometry analysis of *Prmt5* WT vs KO E14.5 FLCs with erythroid differentiation markers CD71 and Ter119 showing a block in differentiation in absence of *Prmt5*. The 5 differentiation stages used for the analysis are according to (Pop et al., 2010). **(G) & (H)** Relative and absolute quantification (respectively) of WT vs KO E14.5 FLCs at stages S0 to S5. **(I)** Giemsa staining of *Prmt5* WT vs KO E14.5 FLCs indicating a lack of differentiated cells (black arrowheads) and an abundance of apoptotic cells (red arrowheads). Scale bars, 20 μm. **(J)** BrdU incorporation assay with *Prmt5* WT vs KO Ter119 negative E14.5 FLCs. Cells at different cell cycle stages are measured by both BrdU incorporation levels and 7AAD staining. Left: representative plots of S0 and S1 cells. Right: Quantification of % cells in G1, S and G2/M phases throughout erythroid differentiation (S0 to S5). **(K)** Same as (A), with E16.5 FLCs. **(L)** Flow cytometry with a Ki67 antibody showing decreased cell proliferation of *Prmt5* KO lineage negative E14.5 FLCs compared to WT. *** *P*<0.001

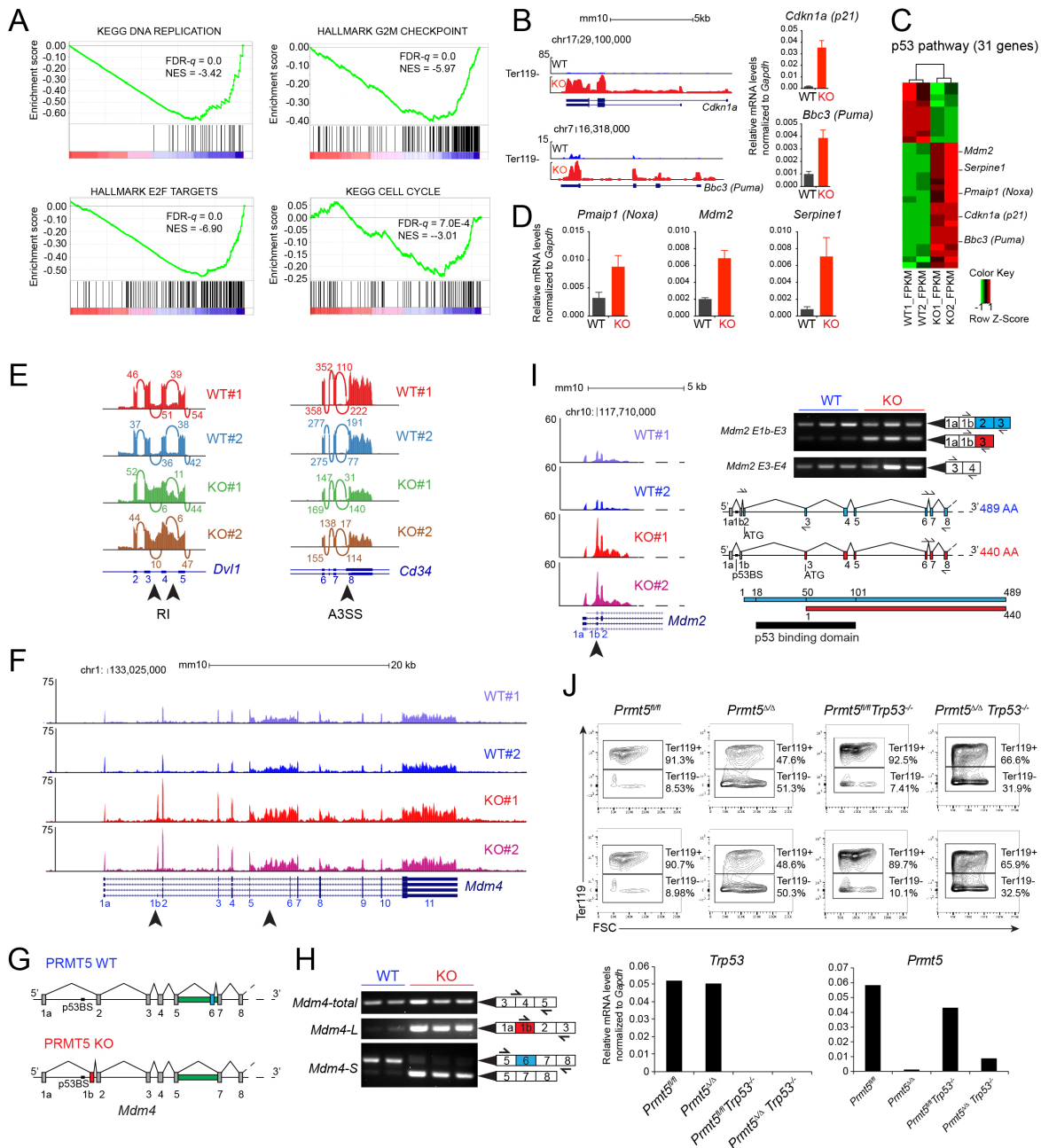


Figure S2. PRMT5 depletion leads to upregulation of the p53 pathway and inhibition of cell cycle progression-associated pathways, and triggers aberrant splicing in hematopoietic progenitors. Related to Figure 3. (A) Gene set enrichment analysis in *Prmt5* WT vs KO Ter119- E14.5 FLCs showing significant downregulation of cell cycle progression associated transcriptional programs (KEGG Cell cycle and DNA replication, HALLMARKS E2F targets, G2M checkpoint). **(B)** Left: UCSC genome tracks showing increasing transcript levels of p53 targets genes *p21* (*Cdkn1a*) and *Puma* (*Bbc3*) in *Prmt5* WT vs KO Ter119- E14.5 FLCs. Right: Corresponding qRT-PCR analysis. **(C)** Heatmap showing the differential expression of the p53 pathway genes (31 genes, manually curated) in *Prmt5* WT vs KO Ter119- E14.5 FLCs. **(D)** qRT-PCR analysis showing increasing levels of p53 targets genes *Noxa* (*Pmaip1*), *Mdm2* and *Serpine1* in *Prmt5* WT vs KO Ter119neg E14.5 FLCs. **(E)** Sashimi plots showing increased intron retention in the *Dvl1* gene and alternative 3' site usage in the *Cd34* gene after *Prmt5* KO in Ter119- E14.5 FLCs. **(F)** UCSC genome tracks showing increased usage of exon 1b and increased intron 5 retention of the *Mdm4* gene in PRMT5 KO Ter119- E14.5 FLCs compared to WT. **(G)** Schematic of the structure of *Mdm4* with differential exon usage between WT and KO cells. **(H)** Semi-quantitative PCR of the indicated transcripts in E14.5 Ter119- PRMT5 WT vs KO FLCs. **(I)** *Mdm2* altered splicing in PRMT5 KO Ter119- E14.5 FLCs compared to WT. Left: UCSC genome tracks showing increased usage of exon 1b in KO cells. Right: Semi-quantitative PCR of the indicated transcripts in E14.5 Ter119neg PRMT5 WT vs KO FLCs. A schematic of the *Mdm2* gene structure is indicated below. Exon1b inclusion generates a transcript coding for a shorter Mdm2 protein with a truncated p53 binding site. **(J)** Top: Flow cytometry analysis of *Prmt5/p53* WT vs double KO E14.5 FLCs with erythroid differentiation marker Ter119 showing a block in differentiation in absence of *Prmt5* that is partially rescued by p53 knockout. Bottom: qRT-PCR analysis showing expression levels of p53 and PRMT5 in *Prmt5^{fl/fl}; Trp53^{-/-}* Vav1-Cre negative (PRMT5 WT) vs Vav1-Cre positive (PRMT5 KO) E14.5 whole FLCs.

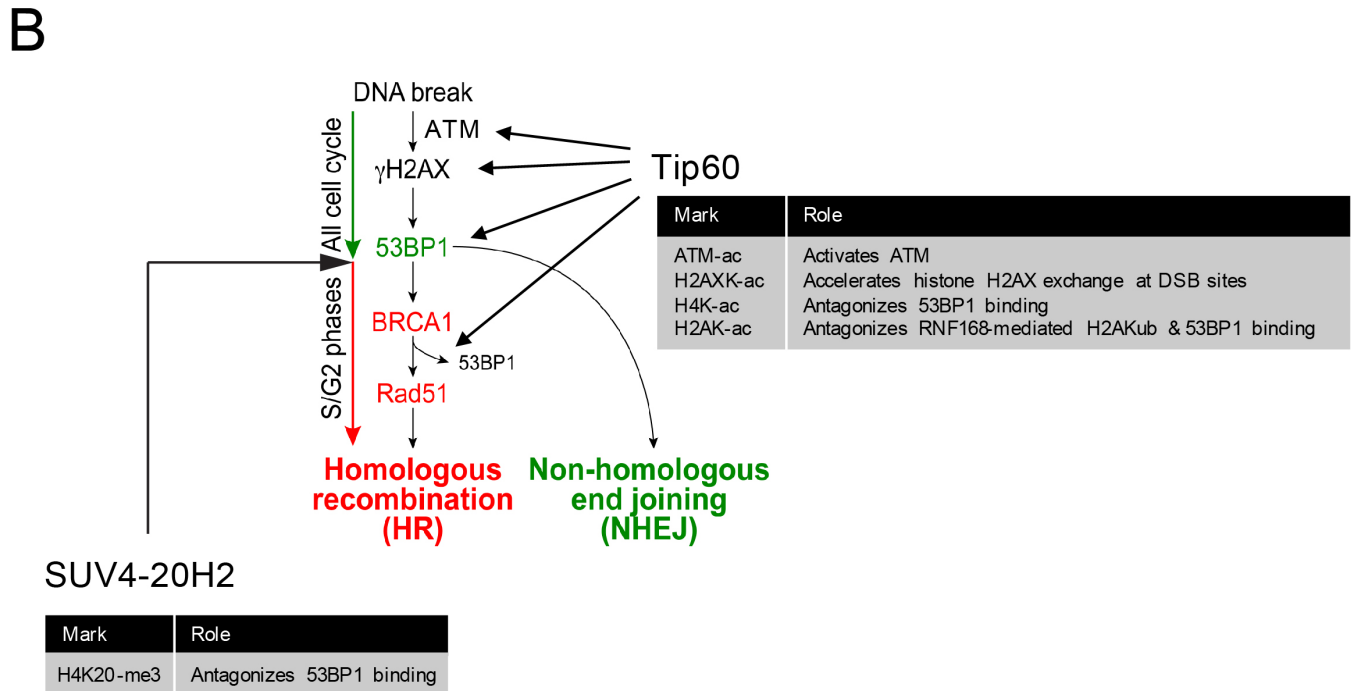
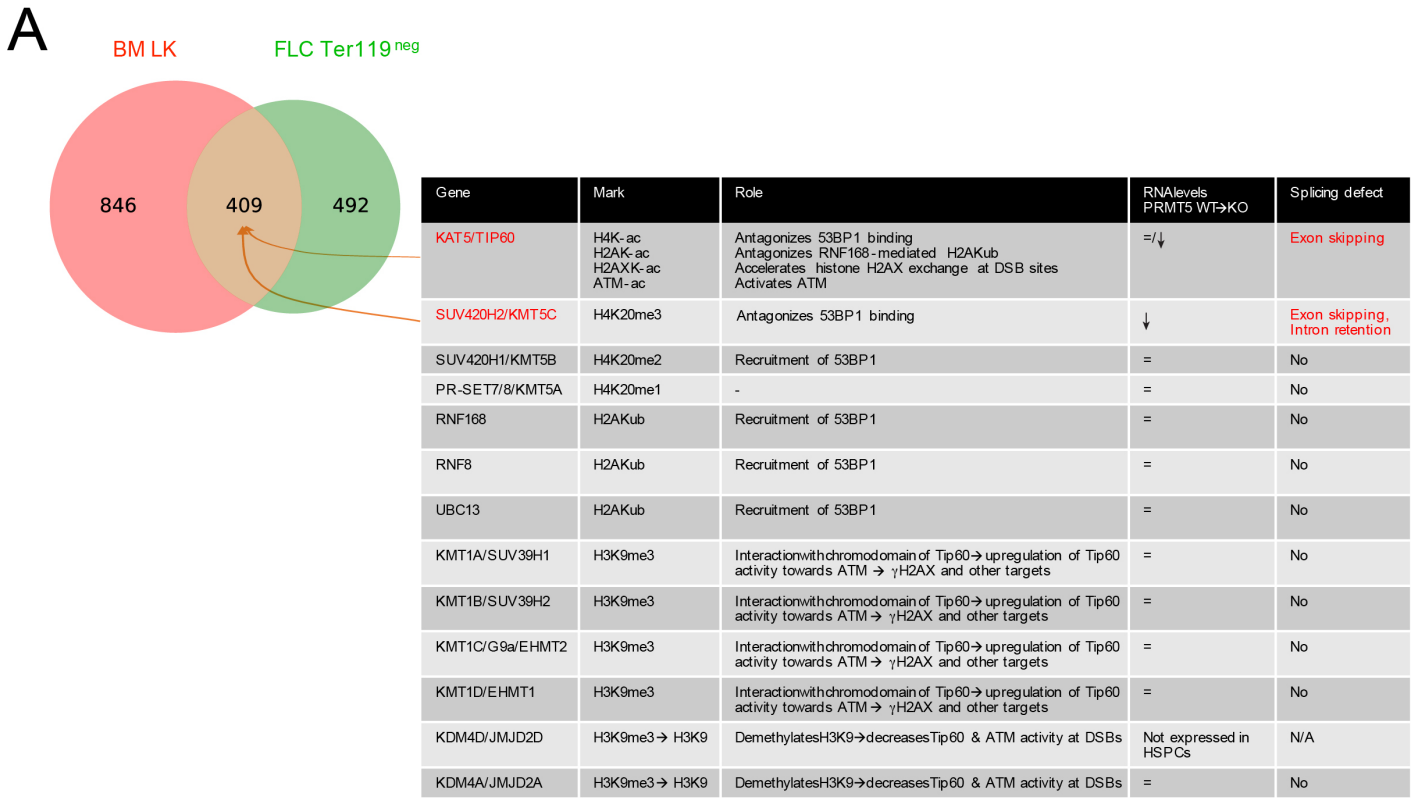


Figure S3. PRMT5 depletion triggers the aberrant splicing of epigenetic factors involved in DNA repair. Related to Figure 3 and Discussion. (A) Left: Venn diagram indicating the overlapping alternate splicing events in adult (LK: lineage negative, Kit positive bone marrow (BM) cells) and fetal liver (Ter119- E14.5 FLCs) hematopoietic progenitor cells. Right: Table listing the epigenetic factors involved in the DNA repair pathways, the marks they deposit on the chromatin, their effects on the DNA repair process, their mRNA levels and the splicing defects affecting them after PRMT5 KO. **(B)** Schematic of the molecular events triggered by a DNA double strand break. The different steps that are impacted by TIP60 and SUV4-20H2 activities are indicated.

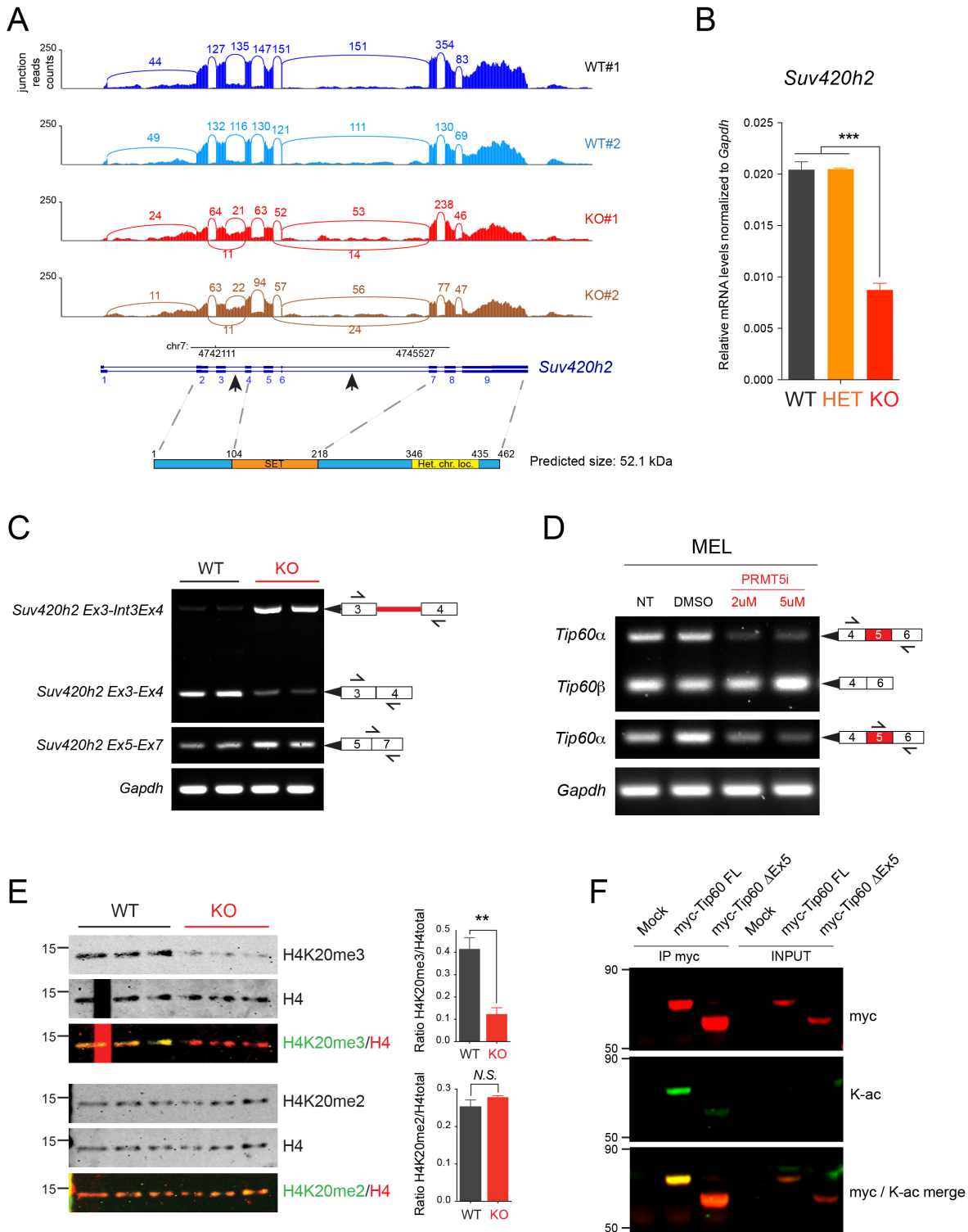


Figure S4. Aberrant splicing of key epigenetic factors affects their activity. Related to Figure 4. (A) Sashimi plot showing the increased intron 3 retention of the gene *Suv420h2* in PRMT5 KO Ter119- FLCs compared to WT cells. Below the Sashimi plot, the structure of *Suv420h2* and of the corresponding protein are shown. **(B)** qRT-PCR analysis showing relative mRNA levels of *Suv420h2* in *Prmt5*^{+/+} (WT), *Prmt5*^{+/fl} (HET), and *Prmt5*^{fl/fl} (KO) *Vav1-Cre*⁺ E14.5 Ter119- FLCs. *** $P < 0.0001$ (Ordinary one-way ANOVA, Adjusted P values). **(C)** Semi-quantitative PCR of the indicated transcripts in E14.5 Ter119- PRMT5 WT vs KO FLCs. **(D)** Semi-quantitative PCR of the indicated transcripts in the mouse leukemia cell line MEL treated with the indicated doses of GSK3186000A for 4 days. **(E)** Multiplex immunoblots with H4K20me2, H4K20me3 and total H4 antibodies in E14.5 Ter119- PRMT5 WT vs KO FLCs, showing decreasing levels of H4K20me3 but no change in H4K20me2 levels after PRMT5 loss. The corresponding quantification of the ratio modified/total H4 is shown on the right. Error bars are SEM of 3 biological replicates. ** $P < 0.001$, N.S. not significant (Student's t -test). **(F)** Immunoprecipitation experiment and multiplex immunoblots with myc-tag (myc) and acetylated lysine (K-ac) antibodies in 293T cells transiently transfected with myc-TIP60 expression vectors (WT vs shorter isoform Δ Ex5). Myc-tagged TIP60 proteins were immunoprecipitated using anti-myc magnetic beads and ran along the corresponding 5% input.

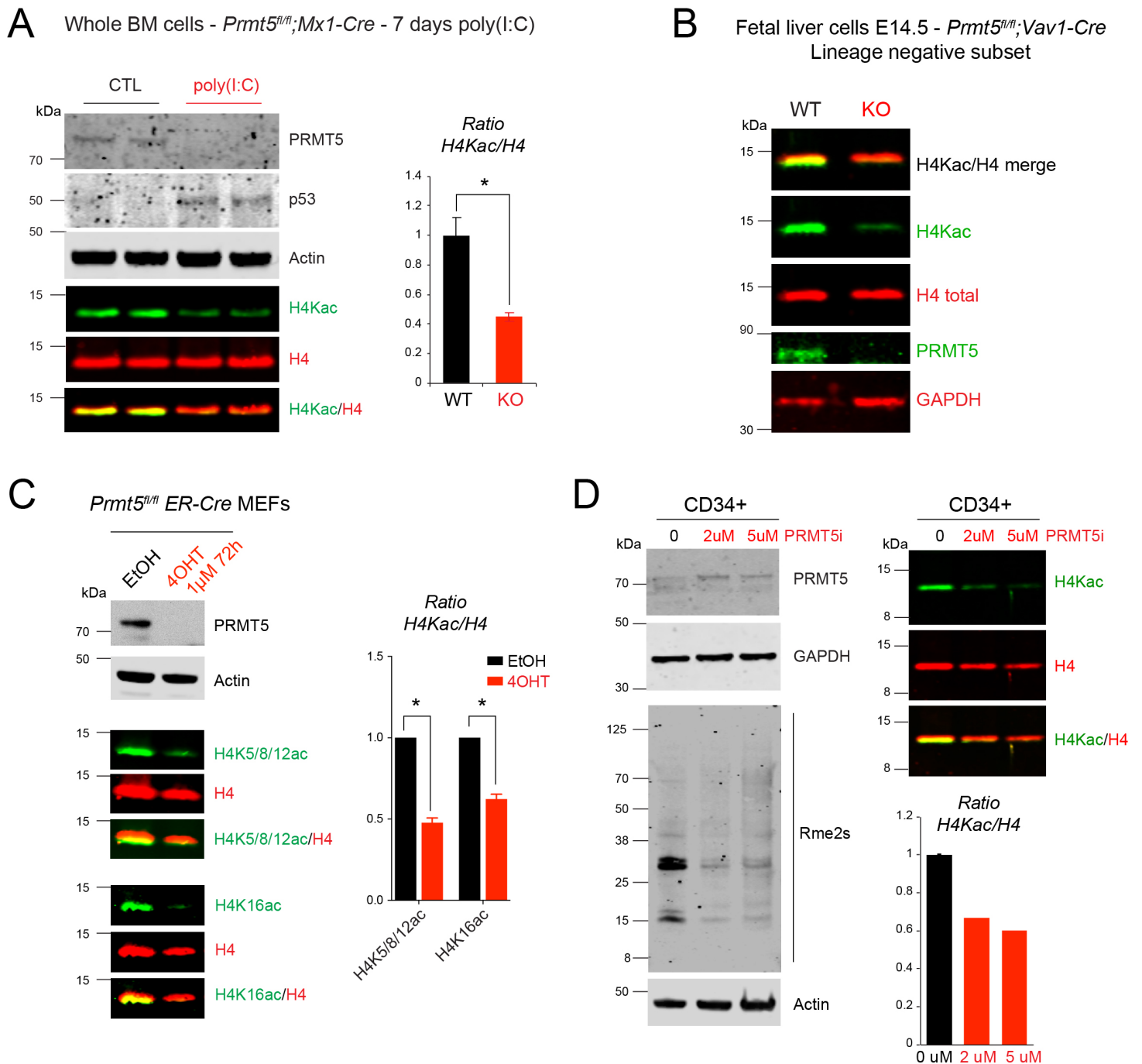


Figure S5. PRMT5 loss leads to aberrant histone H4 acetylation. Related to Figure 4. (A) Left: Multiplex immunoblots with PRMT5, p53, actin, H4Kac, and H4 antibodies in *Prmt5^{fl/fl};Mx1-Cre* mouse whole bone marrow (BM) cells treated with poly(I:C) for 7 days to induce PRMT5 knockout. Right: Quantification of the H4Kac/H4total ratio. Error bars are standard deviation of 3 biological replicates. $*P < 0.05$ (Student's t-test) **(B)** Multiplex immunoblots with H4Kac, H4 total, PRMT5 and GAPDH antibodies showing decreased H4 acetylation in PRMT5 KO E14.5 lineage negative FLCs. **(C)** Left: Multiplex immunoblots with PRMT5, actin, H4K5/8/12ac, H4K16ac and H4 antibodies in *Prmt5^{fl/fl};ER-Cre* mouse embryonic fibroblasts (MEFs) treated with 1 μ M 4-Hydroxytamoxifen (4-OHT) for 4 days. Right: Quantification of the H4Kac/H4total ratio. Error bars are standard deviation of 3 biological replicates. $*P < 0.05$ (Student's t-test) **(D)** Left: Immunoblot with PRMT5, GAPDH, Rme2s and actin antibodies in normal human cord blood derived CD34+ cells treated with the indicated doses of GSK3186000A (PRMT5i) for 4 days. Right: Multiplex immunoblots with H4Kac, and H4 antibodies in CD34+ cells treated with the indicated doses of GSK3186000A for 4 days and quantification of the H4Kac/H4total ratio.

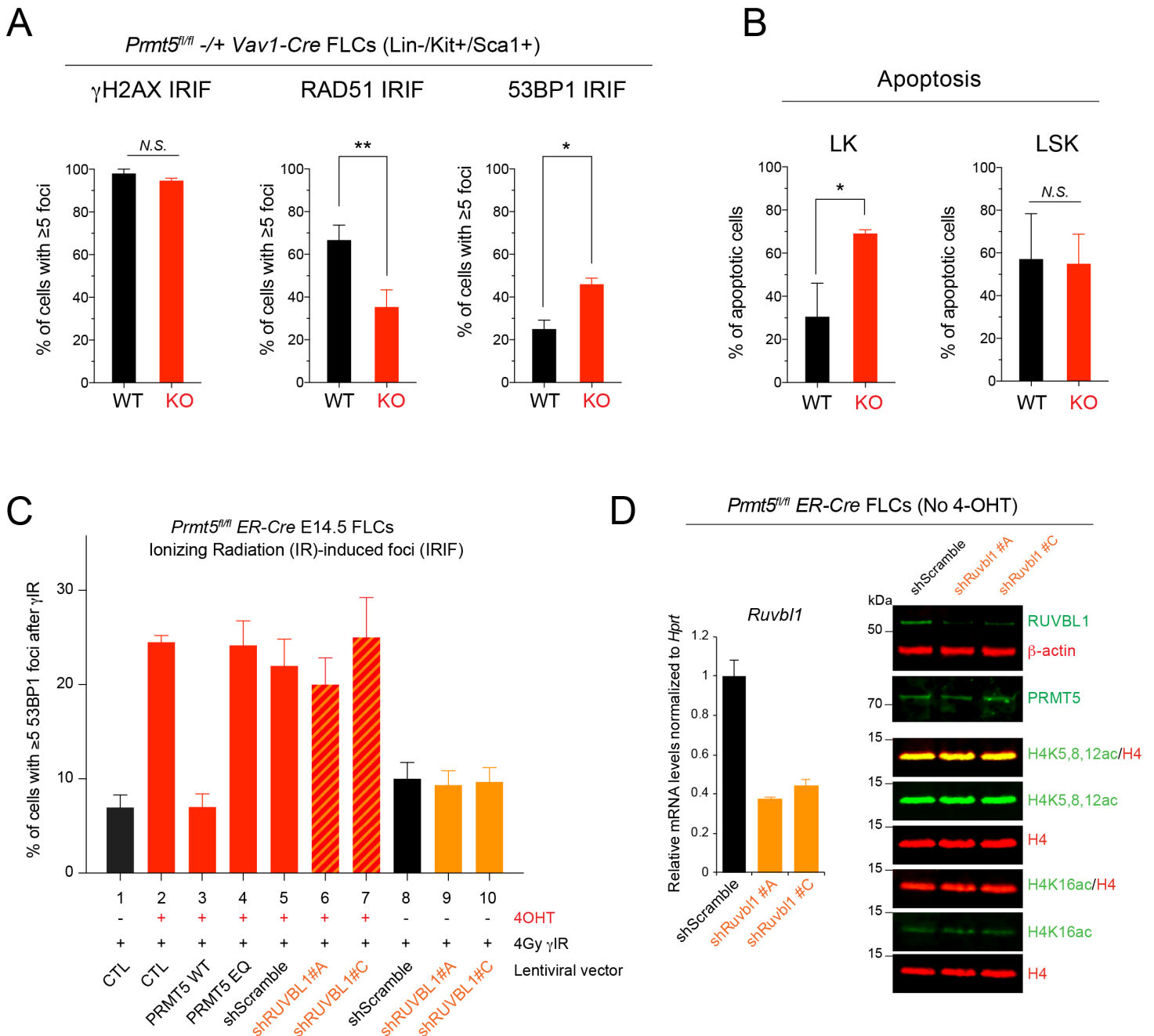


Figure S6. PRMT5 loss affects DNA repair pathways in FLCs. Related to Figure 5 and Figure 6. (A) Immunofluorescence analysis performed with antibodies to γ H2AX, 53BP1 and RAD51 in sorted HSPCs (LSK: lineage negative, Kit+, Sca1+) from PRMT5 WT vs KO E14.5 FLCs, 6h after γ IR-induced DNA damage (10Gy). Quantification of percent of cells with ≥ 5 γ IR-induced foci for the indicated proteins. At least 100 cells were quantified. ** $P < 0.001$, * $P < 0.05$, N.S. not significant (Student's t-test) **(B)** Quantification of percent of apoptotic cells in sorted HSPCs (LK: lin-, Kit+; LSK: lin-, Kit+, Sca1+) from PRMT5 WT vs KO E14.5 FLCs, 6h after γ IR-induced DNA damage (10Gy). At least 100 cells were quantified. * $P < 0.05$, N.S. not significant (Student's t-test). **(C)** Immuno-fluorescence analysis performed with antibodies to γ H2AX and 53BP1 in *Pmt5^{fl/fl};ER-Cre* E14.5 FLCs, before (lanes 1, 8, 9, 10) and after (lanes 2 to 7) 4-OHT treatment (1 μ M for 72h), overexpressing HA-tagged PRMT5 WT (lane 3), or enzymatically dead mutant EQ (lane 4), or shScramble (lanes 5 and 8), shRUVBL1#A (lanes 6 and 9), and shRUVBL1#C (lanes 7 and 10), 6h after γ IR-induced DNA damage (4Gy). Quantification of percent of cells with ≥ 5 γ IR-induced 53BP1 foci from at least two biological replicates. **(D)** Left: qRT-PCR analysis showing relative mRNA levels of *Ruvbl1* in *Pmt5^{fl/fl};ER-Cre* E14.5 FLCs 72h after infection with lentiviral vectors expressing two different shRNAs against *Ruvbl1*. Right: Multiplex immunoblots with RUVBL1, β -actin, PRMT5, H4Kac, H4K16ac and H4 antibodies in *Pmt5^{fl/fl};ER-Cre* mouse fetal liver cells treated with shScramble or shRUVBL1 (#A or #C) for 72 hours in absence of 4-OHT treatment.

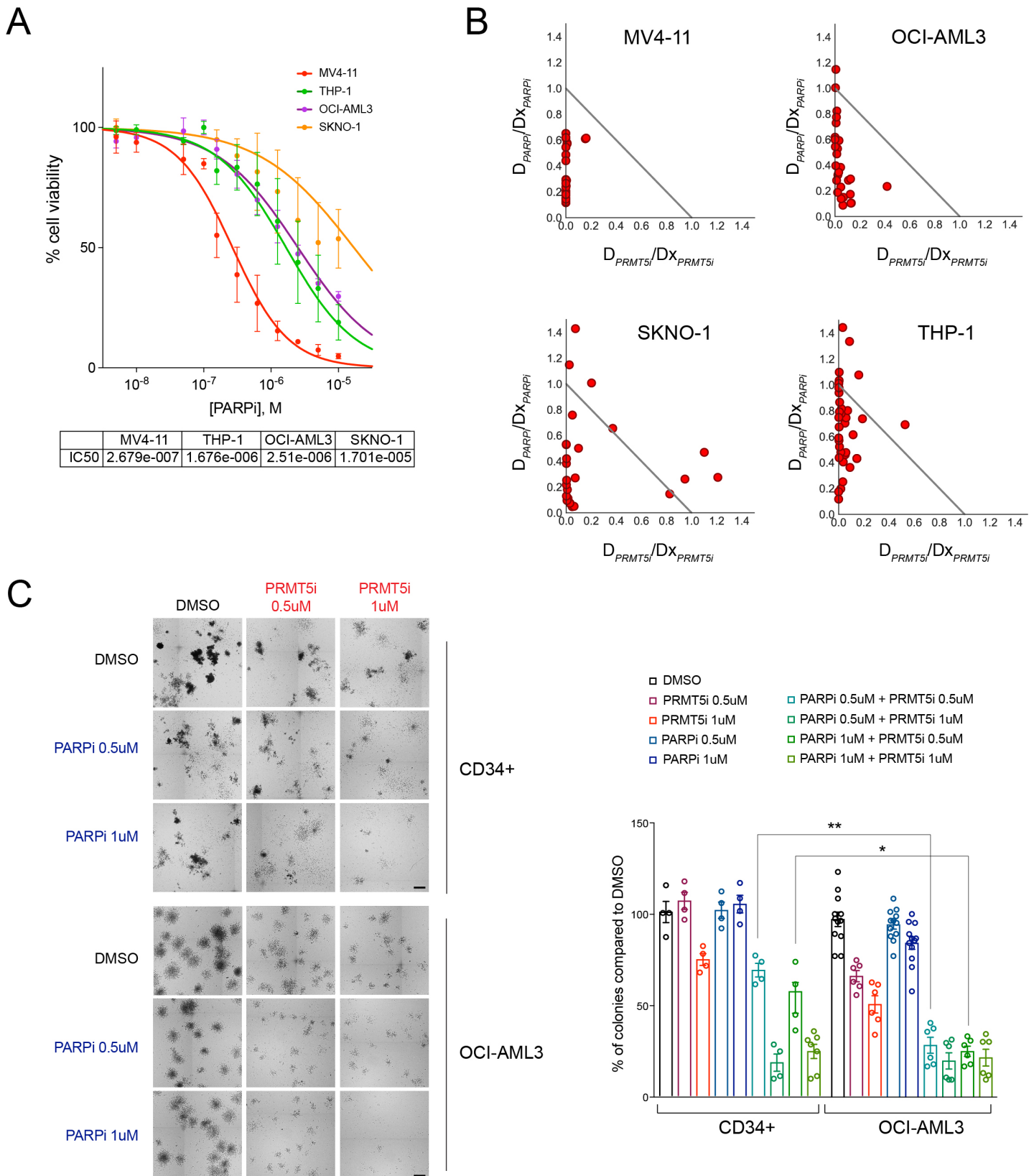


Figure S7. Effect of PRMT5 inhibitor and PARP inhibitor on a panel of AML cell lines. Related to Figure 7. (A) Viability assay assessed with the CellTiter Glo method at day 4 for 4 AML cell lines treated with increasing doses of the PARP inhibitor Olaparib (PARPi). The IC50 for each cell line is indicated below the viability curves. **(C)** Combination index (CI) plots (Chou-Talalay method) of the data shown in Figure 7B. **(D)** Colony forming units after treatment of normal cord blood derived CD34+ cells and the AML cell line OCI-AML3 with DMSO (control), PRMT5 inhibitor (PRMT5i), PARP inhibitor (PARPi) or a combination of PRMT5i and PARPi at the indicated concentrations. Left: representative pictures of colonies on semi-solid methylcellulose media. Scale bar, 1 mm. Right: Quantification of the number of colonies as percent of colonies compared to DMSO, 7 days after plating. ** $P < 0.001$, * $P < 0.05$ (Student's t-test).

Table S1. PRMT5 targeted knockout mouse models. Related to Introduction, Figures 2 and 3, and Discussion.

Model	Targeted tissue	Phenotype	Publication
<i>Prmt5</i> ^{-/-}	Whole organism	No viable homozygous offspring. Early embryonic lethality (>E3.5, <E6.5)	(Tee et al., 2010)
<i>Prmt5</i> ^{fl/fl} ; <i>Nestin-Cre</i>	Precursors of neurons and glia (NSCs), starting at E10.5	DNA damage, p53 induction, cell cycle arrest, apoptosis. Splicing defects	(Bezzi et al., 2013)
<i>Prmt5</i> ^{fl/fl} ; <i>Blimp1-Cre</i>	Primordial germ cells (PGCs), starting at E8.5	DNA damage, p53 induction, cell cycle arrest, apoptosis. Splicing defects	(Kim et al., 2014)
<i>Prmt5</i> ^{fl/fl} ; <i>Blimp1-Cre</i>	Primordial germ cells (PGCs), starting at E8.5	Cell cycle arrest, apoptosis. Splicing defects	(Li et al., 2015)
<i>Prmt5</i> ^{fl/fl} ; <i>Mx1-Cre</i>	Adult hematopoietic stem and progenitor cells (HSPCs). Inducible by poly(IC) injection	p53 induction, cell cycle arrest. Splicing defects	(Liu et al., 2015)
<i>Prmt5</i> ^{fl/fl} ; <i>Pax7-Cre</i> ^{ERT2}	Skeletal muscle stem cells (MuSCs). Inducible by 4OHT treatment	DNA damage, cell cycle arrest, apoptosis. Splicing defects	(Zhang et al., 2015)
<i>Prmt5</i> ^{fl/fl} ; <i>Prx1-Cre</i>	E11.5 limb buds	Apoptosis. Splicing defects	(Norrie et al., 2016)
<i>Prmt5</i> ^{fl/fl} ; <i>Vav1-Cre</i>	Fetal hematopoietic stem and progenitor cells (HSPCs), starting at E11.5	DNA damage, p53 induction, cell cycle arrest, apoptosis. Splicing defects	This manuscript

Table S2. Characteristics of the cell lines used in this study. Related to Figure 1.

Cell line	Viability P5i	Media	Age	Sex	Reported mutations (CCLE/COSMIC/TruSight Myeloid)	FAB	Cytogenetics
CD34+	>10 uM	X-vivo +20% BIT	N/A	N/A	N/A	N/A	N/A
AML-14	0.95 uM	RPMI 10%	68	M	NRAS, TP53	M2	del(5)
HEL	1.1 uM	RPMI 10%	30	M	JAK2V617F homo, TET2, APC, KMT2D, TP53, EP300	M6	complex (5q-)
HL-60	3.9 uM	IMDM 20%	36	F	CDKN2A, NRAS, TP53	M2	
KASUMI-1	2.5 uM	RPMI 20%	7	M	c-KIT, TP53, ASXL1, CBP, RAD21	M2	AML1-ETO
MOLM-13	0.29 uM	RPMI 10%	20	M	FLT3/ITD, CBL, KMT2A, KMT2C, SMARCD1, NF1, SETD1A	M5	MLL-AF9
MV4-11	0.25 uM	RPMI 10%	10	M	FLT3/ITD homo, NPM1	M5	MLL-AF4
NB-4	0.54 uM	RPMI 10%	23	F	KRAS, TP53, ETO, P300, MOZ, ASXL2	M3	PML-RARA
NOMO-1	1.3 uM	RPMI 10%	31	F	KRAS, ASXL1, EP300, SF3B1, TP53, CDKN1B, KMT2C	M5	MLL-AF9
OCI-AML3	1.9 uM	alpha-MEM 20% FBS	57	M	NPM1, NRAS, DNMT3A	M4	
SET-2	1.5 uM	RPMI 20%	71	F	JAK2V617F, TP53, UTX, DNMT3A, SMARCD2	N.D.	
SKNO-1	5.4 uM	RPMI 10% +GM- CSF	22	M	c-KIT, TP53	M2	AML1-ETO
TF-1	1.6 uM	RPMI 10% + IL-3	35	M	TP53, NRAS	M6	
THP-1	>10 uM	RPMI 10%	1	M	CDKN2A, NRAS, TP53, ARID1A, UTX	M5	
U-937	5.7 uM	RPMI 10%	37	M	TP53, WT1, PTEN, ETV6, PTPN11	M5	
UKE-1	0.86 uM	IMDM 10% +HS+HC	59	F	JAK2V617F, IKZF1, EZH2, ETV6, PTPN11, STAG2	N.D.	

Table S3. Aberrant splicing events affecting epigenetic factors. Related to Figure 3.

Gene category/ Gene name	Splicing event	Function
KMT		
KMT1E (SETDB1)	RI	Histone methyltransferase that specifically trimethylates 'Lys-9' of histone H3
KMT5C (SUV4-20H2)	SE	Histone methyltransferase that specifically trimethylates 'Lys-20' of histone H4. H4 'Lys-20' trimethylation represents a specific tag for epigenetic transcriptional repression
KMT6 (EZH2)	SE	Polycomb group (PcG) protein. Catalytic subunit of the PRC2/EED-EZH2 complex, which methylates 'Lys-9' (H3K9me) and 'Lys-27' (H3K27me) of histone H3, leading to transcriptional repression of the affected target gene.
KDM		
KDM5C (Jarid1c)	A5SS	Histone demethylase that specifically demethylates 'Lys-4' of histone H3
KDM8	SE	Histone demethylase required for G2/M phase cell cycle progression. Specifically demethylates dimethylated 'Lys-36' (H3K36me2) of histone H3
KAT		
KAT5 (TIP60)	SE	Component of the NuA4 histone acetyltransferase (HAT) complex, Catalytic subunit
TADA3	RI	Component of the KAT2B (PCAF) complex
ING4	RI	Component of the KAT7 (HBO1) complex, which acetylates H3K14 in vivo
HDAC		
HDAC4	MXE	Deacetylation of lysine residues on the N-terminal part of the core histones (H2A, H2B, H3 and H4)
HDAC10	3ASS	Deacetylation of lysine residues on the N-terminal part of the core histones (H2A, H2B, H3 and H4)
Readers		
MBD5	MXE	Methyl-CpG-binding domain protein 5. Binds to heterochromatin

SUPPLEMENTAL EXPERIMENTAL PROCEDURES

Plasmids

HA-PRMT5 WT and HA-PRMT5 EQ cDNAs were from pcDNA3 vectors previously described (Liu et al., 2011). Myc-tagged TIP60 α , and TIP60 β cDNAs were obtained from Origene (MD, USA). All cDNAs were subcloned into the lentiviral vector pCDH-MSCV-MCS-EF1-GFP with or without their original myc & flag tags (System Biosciences, CA). TIP60 3KR (K104R, K120R, K148R) and TIP60 HATdead (Q377E, G380E) mutants were generated by site-directed mutagenesis and extensively sequenced to ascertain the absence of mutation other than the targeted codons. RUVBL1 mouse shRNA GFP expressing lentiviral vectors were from Origene (Cat# TL509291).

Cell lines and drug treatments

Mouse Embryonic Fibroblasts (MEFs) were isolated by mechanical dissociation and trypsin digestion from E14.5 embryos in cold PBS + 2.5% serum and washed twice in ice-cold PBS 1X. MEFs were grown in DMEM 10% FBS supplemented with Non-Essential Amino Acids (Gibco). CD34+ human cord-blood derived cells were grown in serum-free SFEM II media supplemented with StemSpan™ CD34+ Expansion Supplement (STEMCELL Technologies). Leukemia cell lines were purchased from ATCC or DSMZ and cultured according to provider's instructions. Cell lines were authenticated using short-tandem repeat (STR) assays at the Characterized Cell Line Facility at MD Anderson Cancer Center. All cell lines were grown in the recommended cell culture media at 37°C in 5% CO₂. SKNO-1 cells were supplemented with 10 ng/mL GM-CSF (Peprotech #300-03). THP-1 cells were supplemented with 2-Mercaptoethanol to a final concentration of 0.05 mM (Gibco). Cells were treated with the indicated doses of drugs for the indicated periods of time. GlaxoSmithKline provided GSK3186000A (compound n°14) (Duncan et al., 2016) for purposes of this research. GSK3186000A was discovered through a Research Collaboration and License Agreement between GlaxoSmithKline and Epizyme, Inc. GlaxoSmithKline has exclusive worldwide rights to GSK3186000A. Stock solutions were prepared in DMSO and stored at -20°C. The PARP inhibitor Olaparib was purchased from LC labs (O-9201). Final DMSO concentrations were kept below 0.1%. Cell viability was assessed by a CellTiter-Glo Luminescent Cell Viability Assay (Promega) at the indicated time points, according to the manufacturer's protocol.

CTRP v2.1 data analysis

Cancer Therapeutic Research Portal v2.1 compound sensitivity data was obtained from <http://portals.broadinstitute.org/ctrp/> and (Rees et al., 2015). Briefly, pairwise spearman correlations were generated comparing all CTRP compounds to PRMT5i sensitivity using area under the curve (AUC) drug response measurements across 12 AML cell lines. Annotation classes were generated and filtered for non-degenerative or single compound groups. Positive and negative compound group enrichment was determined using an extension of the minimum hypergeometric test (XL-mHG) as described in (Eden et al., 2007) and (Wagner, 2015).

Fetal liver isolation and cell sorting

Timed breedings were set up in order to isolate embryo fetal liver cells at embryonic day E14.5 and E16.5. Pregnant females were sacrificed according to the University of Miami-IACUC guidelines. FLCs were isolated by mechanical dissociation in cold PBS + 2.5% serum and washed twice in ice-cold PBS 1X. 1x10⁵ cells were used for cytopsin preparation with Thermo Shandon CytoSpin 3. Slides were air-dried overnight and stained with Giemsa (Thermo Scientific #3300). The remainder of the cells was stained for flow cytometric analysis and cell sorting. Cells were incubated for 20 minutes on ice with the antibodies cocktails diluted in PBS/2%FBS. Antibodies used are listed in [Table S4](#). Immunofluorescence was measured on an LSR-Fortessa-HTS (BD Biosciences, CA) or a FACS Canto-II and data analyzed using FlowJo (Tree Star, CA). Cells were sorted using a FACS Aria III cell sorter at the Sylvester Comprehensive Cancer Center Flow Cytometry Facility at the University of Miami. Alternatively, for western blot, lineage⁻ cells were isolated from mouse fetal liver using a Lineage Cell Depletion Kit (Miltenyi Biotec, # 130-090-858).

For cell cycle analysis, BrdU (100 μ L of 10 mg/ml) was injected intra-peritoneally to pregnant mice and embryos were harvested 60 min later. BrdU incorporation was detected using BrdU flow kit (BD Biosciences).

Colony formation assay

Prmt5^{fl/fl};ER-Cre E14.5 fetal liver cells were harvested at day 0 and expanded for 3 days in complete growth media (X-Vivo 15 (Lonza, #04-744Q), mIL-3 (Peprotech #213-13) 10 ng/mL, mIL-6 (Peprotech #200-06) 20 ng/mL, mSCF (Peprotech #300-07B) 100ng/mL, 10% FBS, penicillin/streptomycin antibiotics). Cells were then

transduced with GFP-expressing lentiviral vectors at day 3, and GFP-positive cells were sorted at day 6. Cells were left in liquid culture overnight with or without 1 μ M 4-Hydroxytamoxifen (4-OHT, Sigma #H7904) before 1) plating in methylcellulose semi-solid media supplemented with 1 μ M 4-OHT or ethanol as control (MethoCult™ GF M3434, STEMCell Technologies) or 2) irradiation (4Gy) and immunofluorescence (see below) 6h after irradiation. One tenth of cells were kept in liquid culture for 3 more days and used for preparing mRNA and cDNA to assess the knockdown of endogenous PRMT5 after 4-OHT treatment and the expression levels of ectopic PRMT5 and TIP60. GFP+ colonies were scored after 2 weeks using an Olympus IX70 inverted fluorescence microscope.

CD34+ human cord-blood derived cells (purchased from STEMCell Technologies), OCI-AML3 and MV4-11 AML human cell lines were plated in methylcellulose semi-solid media supplemented with DMSO (control), PRMT5 inhibitor GSK3186000A, PARP inhibitor Olaparib, or a combination of both (MethoCult™ H4435 Enriched, STEMCell Technologies). Scoring of colonies was performed after 7 days using the automated and standardized colony counting machine STEMvision™ (STEMCell Technologies).

Western Blotting

Cells were lysed in Cell Lysis Buffer or RIPA lysis buffer (Cell Signaling Technology, #9803 and # 9806), supplemented with Protease Inhibitor Cocktail tablet (Roche Applied Science) and 1mM PMSF (Sigma). After a 10 minutes incubation on ice, protein lysates were sonicated at 4°C with a Bioruptor® Plus (Diagenode), centrifuged at 4°C and 15,000 rpm for 5 minutes, and the supernatants were collected. Total protein concentration was quantified using BCA Protein Assay Kit (ThermoFisher Scientific) according to the manufacturer's instructions. The proteins were then eluted in Sample Buffer with reducing agent DTT. For Western Blots, the samples were boiled at 95°C for 5 minutes, equal amounts of the proteins were loaded for SDS PAGE. Proteins were transferred to a nitrocellulose or a PVDF membrane and incubated with primary antibody at 4°C overnight in PBS/Tween 5% milk. Antibodies used are listed in [Table S4](#). Proteins were detected with either of the following detection systems:

- 1) Chemiluminescent detection of horseradish peroxidase-conjugated secondary antibodies was performed using the Immobilon Western Chemiluminescent HRP Substrate (EMD Millipore) according to the manufacturer's instructions.
- 2) Infrared fluorescent IRDye® secondary antibodies (LI-COR, NE) were detected using an Odyssey CLx imager (LI-COR, NE). The LI-COR Image Studio software was used to quantify the western-blot data.

Neutral comet assay of double-strand DNA breaks

Single-cell comet electrophoresis was performed using the Trevigen CometAssay® kit (Trevigen) according to manufacturer's instructions. Lin- cells were sorted by FACS and treated with the agents described for the durations indicated. Approximately 2x10⁵ cells were resuspended in 0.1% low-melting point agarose in 1x PBS. 50 μ l of the cell suspension was pipetted onto designated areas of CometSlides® and allowed to solidify for 10 minutes at 4°C. Cells were lysed in CometAssay® Lysis Solution for 1 hour in the dark at 4°C. Samples were immersed in 1x Neutral Electrophoresis Buffer (NED; Tris-acetate pH 9.0) for 30 minutes at 4°C and then transferred to an electrophoresis unit. Slides were aligned equidistant from electrodes. The electrophoresis unit was filled with 1x NEB to a height of 0.5 cm above the slides, and a constant current of 1.0V/cm, measured between electrodes, was applied for 60 minutes at 4°C. Slides were removed from the unit and placed flat in DNA precipitation solution (1M NH₄Ac in 95% ethanol) for 30 minutes at room temperature in the dark. Afterward, slides were transferred into 70% ethanol for an additional 30 minutes at room temperature in the dark. Samples were subsequently dried at room temperature, in the dark, overnight. Samples were stained the following day with 1x SYBR® Green I stain (Invitrogen) diluted 1:10,000 in Tris-EDTA buffer pH 7.5. Comets were visualized at 10x magnification using an Eclipse Ti microscope (Nikon, Japan) equipped with an Andor Zyla 5.5 digital camera (Andor Technology Ltd, UK). Images were captured using the NIS Elements AR v. 4.30 software (Nikon, Japan). Percent tail DNA for 50 nuclei per experimental point was determined using Image J software (NIH) with the Comet Assay plug-in (original macro from Herbert M. Geller, NIH, 1997, later development by Robert Bagnell, 2011, UNC-CH). Statistical significance of comet assay results was determined using a nonparametric Mann-Whitney U test.

In vitro acetylation

In vitro acetylation was performed as previously described (Kuninger et al., 2007). Briefly, purified or recombinant proteins were incubated at 30°C for 1h in acetyl-transferase assay buffer (50 mM Tris-Cl, pH 8, 10% glycerol, 10 mM butyric acid, 0.1 mM EDTA, 1 mM DTT, 1 mM PMSF) with 10 μ M Acetyl-CoA (Sigma-Aldrich). Recombinant histones were purchased from NEB. Myc-tagged full-length TIP60 aka TIP60 α , and TIP60 Δ Ex5

aka TIP60 β were overexpressed in 293T cells using plasmids from Origene (MR223769 and MR230030, respectively) and purified using Anti-c-Myc Magnetic Beads (ThermoFisher Scientific #88842). Reactions were stopped by addition of SDS-PAGE sample buffer.

RNA extraction and quantitative RT-PCR

RNA was isolated from mouse FLCs or from cell lines with the RNeasy Plus Micro Kit (Qiagen). Equal amounts of RNA were used for RT reaction according to manufacturer's instructions (qScript™ cDNA SuperMix, Quanta Biosciences). Quantitative PCR (qPCR) was performed with the SYBR® Green PCR Master Mix or the TaqMan Universal PCR Master Mix (Applied Biosystems) and a "7500 Real-Time PCR System" thermocycler (Applied Biosystems). Gene expression levels were normalized to the reference gene *Gapdh* or *Hprt*.

Primer pairs and Taqman probes used for PCR were from ThermoFisher Scientific and are listed in [Table S5](#).

RNA-seq and differential expression analysis

For sorted E14.5 Ter119-/+ mouse FLCs from *Prmt5^{fl/fl};Vav1-Cre⁺ or -* mice, RNA was isolated with TRIzol (ThermoFisher Scientific) and RNA-Seq library prep was carried out using the Illumina TruSeq Total Stranded kit with Ribo-Zero rRNA reduction following manufacturer's standard protocol without modification. 500 ng of total RNA was used as input with RNA quality assessed using Agilent Bioanalyzer 2100 Nano 6000 lab-on-chip. Library quantification and balancing was done using Kapa Biosciences Library Quantification (Complete, K4824) run on a Roche LC480 LightCycler. Samples were loaded and run on an Illumina NextSeq 500 per manufacturer's standard protocol. For Lin⁻/Kit⁺ adult BM cells from *Prmt5^{fl/fl};Mx1-Cre⁺* mice, RNA was isolated 7 days after poly(I:C) treatment, using the RNeasy Plus Micro Kit (Qiagen). RNA-Seq library prep was carried out using the Illumina TruSeq Total Stranded kit with Ribo-Zero rRNA reduction following manufacturer's standard protocol without modification. Samples were loaded and run on an Illumina HiSeq 2000 per manufacturer's standard protocol. Data was uploaded directly to Illumina BaseSpace for base-calling and demultiplexing.

Reads were aligned to the GRCm38/mm10 build of the *Mus musculus* genome using the STAR aligner (v2.5.2b) and expected transcript counts were determined using RSEM (v1.2.28) (Dobin et al., 2013). Overall differential gene expression was analyzed using DESeq2 (Love et al., 2014). Genes with an FDR adjusted q value below 0.05 and exhibiting a 2-fold change in expression were considered "differential".

Heatmaps were generated from differentially expressed genes, calculated using Euclidean distances on variance stabilized counts, and clustered using complete-linkage. Pathway enrichment of the top six clusters were performed for GO Biological Process (2017), GO Molecular Process (2017), and KEGG (2016) using EnrichR (Kuleshov et al., 2016). The combined scores were calculated with Enrichr (Kuleshov et al., 2016). GSEA (Subramanian et al., 2005) was also used to identify GO terms over-represented by genes with significant differential expression or alternative splicing (see below). Connectivity graphs were generated with Cytoscape version 3.6.0 (<http://www.cytoscape.org/>) and the AutoAnnotate plugin using the Community Cluster Annotation set.

Splicing analysis

To identify differential alternative splicing (AS) events between WT and KO mice, the RNAseq data was reanalyzed using a multivariate analysis of transcript splicing with replicates (rMATS v3.2.5) (Shen et al., 2014). For each AS event, reads mapped to the splice junctions and the exon body were used as the input for rMATS. Briefly, reads were trimmed and filtered to 100bp and aligned using STAR aligner to GRCm38/mm10 and annotated with Ensembl GRCm38/mm10. Events with q-value < 0.05 and >20% inclusion after filtering out low expressing genes (lower quartile of base mean expected count) were considered significant. Differences in skipped exons, retained introns, mutually exclusive exons, and alternative 3' and 5' splice sites were analyzed. The ASPIRE index was calculated with AltAnalyze 2.1.0 (Emig et al., 2010).

For RNA splicing validation, primers were designed using Primer3plus (<http://www.bioinformatics.nl/cgi-bin/primer3plus/primer3plus.cgi>). PCRs were performed using the following program: 95°C for 5 minutes, 35 cycles of denaturation at 95°C for 45s, annealing at 58°C for 30s and elongation at 72°C for 40s and a final elongation temperature of 72°C for 4 minutes and 4°C holding temperature. PCR products were run in a range of 2% to 3% agarose gels stained with Midori green DNA staining dye (Bulldog Bio, NH). Bands were visualized using a Chemidoc XRS+ system (BioRad). Band intensities were quantified using Image Lab software (BioRad).

Table S4. Antibodies used in this study. Related to Experimental Procedures.

Antibody	Isotype	Manufacturer	Cat. #
PRMT5	Rabbit	Millipore	07-405
PRMT5	Goat	Santa Cruz	sc-22132
p53	Rabbit	Leica	CM5
p21	Mouse	BD Biosciences	SXM30
GAPDH	Rabbit	Santa Cruz	sc-25778
GAPDH	Mouse	Abcam	ab8245
β -actin	Rabbit	Santa Cruz	sc-130656
β -actin	Mouse	Sigma-Aldrich	A5441
Caspase-3	Rabbit	Cell Signaling	#9665
TIP60	Rabbit	Gift from Bruno Amati	-
TIP60	Rabbit	Cell Signaling	#12058
SmD3	Rabbit	Abcam	ab121129
Arg-me2s (Rme2s)	Rabbit	Cell Signaling	#13222
RAD51	Rabbit	BioAcademia	70-001
53BP1	Rabbit	Novus Biologicals	NB100-304
Flag-Tag	Mouse	Sigma-Aldrich	F3165
Myc-tag	Mouse	Santa Cruz	sc-40
HA-tag	Rabbit	Abcam	ab128131
H3	Goat	Santa Cruz	sc-8654
H3	Mouse	Abcam	ab24834
H3K27me3	Rabbit	Cell Signaling	#9733
H4	Mouse	Abcam	ab17036
H4K5,8,12,16ac	Rabbit	Diagenode	C15410024
H4K5,8,12ac	Rabbit	Diagenode	C15410021
H4K16ac	Rabbit	Diagenode	C15410300
H4K16ac	Rabbit	Active Motif	39167
H4K20me2	Rabbit	Epigentek	A-4047-050
H4K20me3	Rabbit	Cell Signaling	#5737
H2A	Mouse	Cell Signaling	#3636
γ H2AX	Mouse	Millipore	05-636
H2AX-K5ac	Rabbit	Millipore	AB10020
H2AK15ac	Rabbit	Epigentek	A68385-100
H2AX	Rabbit	Cell Signaling	#7631
K-acetyl (K-ac)	Rabbit	Cell Signaling	#9441
RUVBL1	Rabbit	ThermoFisher Scientific	PA5-29278
Anti-Mouse IgG Antibody, Alexa Fluor 594 Conjugated	Donkey	ThermoFisher Scientific	A21203
Anti-Rabbit IgG Antibody, Alexa Fluor 488 Conjugated	Donkey	ThermoFisher Scientific	A21206
Anti-Mouse IgG Antibody, IRDye® 680RD Conjugated	Donkey	Li-Cor Biosciences	926-68072
Anti-Rabbit IgG Antibody, IRDye® 680RD Conjugated	Donkey	Li-Cor Biosciences	926-68073
Anti-Mouse IgG Antibody, IRDye® 800CW Conjugated	Donkey	Li-Cor Biosciences	926-32212
Anti-Rabbit IgG Antibody, IRDye® 800CW Conjugated	Donkey	Li-Cor Biosciences	926-32213
Anti-Goat IgG Antibody, IRDye® 680RD Conjugated	Donkey	Li-Cor Biosciences	926-68074
Biotin-CD3	Hamster	BD Biosciences	553059
Biotin-CD4	Rat	BD Biosciences	553728
Biotin-CD5	Rat	BD Biosciences	553019
Biotin-CD8	Rat	BD Biosciences	553029
Biotin-CD127	Rat	BD Biosciences	555288
Biotin-Gr-1	Rat	BD Biosciences	553125
Biotin-CD45R/B220	Rat	BD Biosciences	553086
Biotin-Ter119	Rat	BD Biosciences	553672
Streptavidin APC-Cy7	-	BD Biosciences	554063
Streptavidin PerCP-Cy5.5	-	Biologend	405214
BV421-CD45	Rat	BD Biosciences	566095
PE-Cy7-Sca1	Rat	eBioscience	25-5981
APC-Mac1/CD11b	Rat	eBioscience	17-0112
APC-Kit	Rat	BD Biosciences	553356
Pacific Blue-Ki67	Rat	eBioscience	48-5698
PE-CD71	Rat	Biologend	113808
APC-Ter119	Rat	Biologend	116212
FITC-Ter119	Rat	Biologend	116206

Table S5. Taqman probes and primers used in this study. Related to Experimental Procedures.

Taqman probes

Target	Ref. #
<i>Prmt5</i>	Mm00550472_m1
<i>Trp53</i>	Mm01731290_g1
<i>Cdkn1a/p21</i>	Mm04205640_g1
<i>Bbc3/Puma</i>	Mm00519268_m1
<i>Pmaip1/Noxa</i>	Mm00451763_m1
<i>Mdm2</i>	Mm01233136_m1
<i>Serpine1</i>	Mm00435860_m1
<i>Kat5 (Tip60)</i>	Mm01231512_m1
<i>Kmt5c (Suv4-20h2)</i>	Mm00525366_m1
<i>Ruvbl1</i>	Mm04203863_g1
<i>Gapdh</i>	Mm99999915_g1
<i>Hprt</i>	Mm01545399_m1

Primer pairs

Target		Sequence
<i>Kat5 Ex4</i>	F	GAGGCCAAGACACCTACCAA
<i>Kat5 Ex5</i>	F	GGGAAGACCTTGCCAATCC
<i>Kat5 Ex6</i>	R	GTGAAACCACCTCCACCTTC
<i>Mdm4 Ex3/4</i>	F	AGTCAGGTGCGGCCAAAA
<i>Mdm4 Ex5</i>	R	CCCAAAAGATCTCCACCACA
<i>Mdm4 Ex1b</i>	F	AAATGCAGTGCAGGCCTTAG
<i>Mdm4 Ex3</i>	R	GCTGCATGCAAAATCTTCAA
<i>Mdm4 Ex5</i>	F	TGTGGTGGAGATCTTTTGGG
<i>Mdm4 Ex8</i>	R	TCAGTTCTTTTTCTGGGATTGG
<i>Mdm2 Ex1b</i>	F	GGACCCTCTCGGATCACC
<i>Mdm2 Ex3</i>	R	CGCTCCAACGGACTTTAACA
<i>Mdm2 Ex3</i>	F	GCCAATGTGCAATACCAACA
<i>Mdm2 Ex4</i>	R	CTCTTTCATAGTGTAAGTGTGCTTTT
<i>Suv4-20h2 Ex3</i>	F	GACAACACCACCTTCGTTCA
<i>Suv4-20h2 Ex4</i>	R	CGCGGAGGTAGCAGAAAAT
<i>Suv4-20h2 Ex5/7</i>	F	CAACCATGTTTGTGCCCTCA
<i>Suv4-20h2 Ex7</i>	R	AAGCCCTCACCATAGAAGCA
<i>Gapdh</i>	F	AAGGGCTCATGACCACAGTC
<i>Gapdh</i>	R	GGATGCAGGGATGATGTTCT
<i>TIP60 K104R mutagenesis</i>	F	GCCAGGCCAGCGGGAGGACCTTGCCAATCCCG
	R	CGGGATTGGCAAGGTCTCCCGCTGGCCTGGGC
<i>TIP60 K120R mutagenesis</i>	F	CGCTTCAACCTGCCAGAGAGCGGGAGGCCATC
	R	GATGGCCTCCCGCTCTGGGCAGGTTGAAGCG
<i>TIP60 K148R mutagenesis</i>	F	AACCACCGCTCAACGAGACGGAAGGTGGAGGTG
	R	CACCTCCACCTTCCGTCTCGTTGAGCGGTGGTT
<i>TIP60 Q377E G380E mutagenesis</i>	F	ACTCTGCCTCCCTACGAGCGCCGGGAGTATGGC
	R	GCCATACTCCCGCGCTCGTAGGGAGGCAGAGT

SUPPLEMENTAL REFERENCES

- Bezzi, M., Teo, S.X., Muller, J., Mok, W.C., Sahu, S.K., Vardy, L.A., Bonday, Z.Q., and Guccione, E. (2013). Regulation of constitutive and alternative splicing by PRMT5 reveals a role for Mdm4 pre-mRNA in sensing defects in the spliceosomal machinery. *Genes Dev* 27, 1903–1916.
- Dobin, A., Davis, C.A., Schlesinger, F., Drenkow, J., Zaleski, C., Jha, S., Batut, P., Chaisson, M., and Gingeras, T.R. (2013). STAR: ultrafast universal RNA-seq aligner. *Bioinformatics* 29, 15–21.
- Duncan, K.W., Rioux, N., Boriack-Sjodin, P.A., Munchhof, M.J., Reiter, L.A., Majer, C.R., Jin, L., Johnston, L.D., Chan-Penebre, E., Kuplast, K.G., et al. (2016). Structure and Property Guided Design in the Identification of PRMT5 Tool Compound EPZ015666. *ACS Med. Chem. Lett.* 7, 162–166.
- Emig, D., Salomonis, N., Baumbach, J., Lengauer, T., Conklin, B.R., and Albrecht, M. (2010). AltAnalyze and DomainGraph: analyzing and visualizing exon expression data. *Nucleic Acids Res* 38, W755–W762.
- Kim, S., Günesdogan, U., Zylicz, J.J., Hackett, J.A., Cougot, D., Bao, S., Lee, C., Dietmann, S., Allen, G.E., Sengupta, R., et al. (2014). PRMT5 Protects Genomic Integrity during Global DNA Demethylation in Primordial Germ Cells and Preimplantation Embryos. *Mol Cell* 56, 564–579.
- Kuleshov, M.V., Jones, M.R., Rouillard, A.D., Fernandez, N.F., Duan, Q., Wang, Z., Koplev, S., Jenkins, S.L., Jagodnik, K.M., Lachmann, A., et al. (2016). Enrichr: a comprehensive gene set enrichment analysis web server 2016 update. *Nucleic Acids Res* 44, W90–W97.
- Kuninger, D., Lundblad, J., Semirale, A., and Rotwein, P. (2007). A non-isotopic in vitro assay for histone acetylation. *Journal of Biotechnology* 131, 253–260.
- Li, Z., Yu, J., Hosohama, L., Nee, K., Gkoutela, S., Chaudhari, S., Cass, A.A., Xiao, X., and Clark, A.T. (2015). The Sm protein methyltransferase PRMT5 is not required for primordial germ cell specification in mice. *Embo J* 34, 748–758.
- Liu, F., Cheng, G., Hamard, P.-J., Greenblatt, S., Wang, L., Man, N., Perna, F., Xu, H., Tadi, M., Luciani, L., et al. (2015). Arginine methyltransferase PRMT5 is essential for sustaining normal adult hematopoiesis. *J Clin Invest* 125, 3532–3544.
- Liu, F., Zhao, X., Perna, F., Wang, L., Koppikar, P., Abdel-Wahab, O., Harr, M.W., Levine, R.L., Xu, H., Tefferi, A., et al. (2011). JAK2V617F-mediated phosphorylation of PRMT5 downregulates its methyltransferase activity and promotes myeloproliferation. *Cancer Cell* 19, 283–294.
- Love, M.I., Huber, W., and Anders, S. (2014). Moderated estimation of fold change and dispersion for RNA-seq data with DESeq2. *Genome Biol* 15, 550.
- Norrie, J.L., Li, Q., Co, S., Huang, B.-L., Ding, D., Uy, J.C., Ji, Z., Mackem, S., Bedford, M.T., Galli, A., et al. (2016). PRMT5 is essential for the maintenance of chondrogenic progenitor cells in the limb bud. *Development* 143, 4608–4619.
- Pop, R., Shearstone, J.R., Shen, Q., Liu, Y., Hallstrom, K., Koulunis, M., Gribnau, J., and Socolovsky, M. (2010). A key commitment step in erythropoiesis is synchronized with the cell cycle clock through mutual inhibition between PU.1 and S-phase progression. *Plos Biol* 8.
- Shen, S., Park, J.W., Lu, Z.-X., Lin, L., Henry, M.D., Wu, Y.N., Zhou, Q., and Xing, Y. (2014). rMATS: robust and flexible detection of differential alternative splicing from replicate RNA-Seq data. *Proc Natl Acad Sci U S A* 111, E5593–E5601.
- Subramanian, A., Tamayo, P., Mootha, V.K., Mukherjee, S., Ebert, B.L., Gillette, M.A., Paulovich, A., Pomeroy, S.L., Golub, T.R., Lander, E.S., et al. (2005). Gene set enrichment analysis: a knowledge-based approach for interpreting genome-wide expression profiles. *Proc Natl Acad Sci USA* 102, 15545–15550.

Tee, W.-W., Pardo, M., Theunissen, T.W., Yu, L., Choudhary, J.S., Hajkova, P., and Surani, M.A. (2010). Prmt5 is essential for early mouse development and acts in the cytoplasm to maintain ES cell pluripotency. *Genes Dev* 24, 2772–2777.

Zhang, T., Günther, S., Looso, M., Künne, C., Krüger, M., Kim, J., Zhou, Y., and Braun, T. (2015). Prmt5 is a regulator of muscle stem cell expansion in adult mice. *Nat Comms* 6, 7140.